OCEANSAT-II-UP/SCATT-1/SAC-2007

ALGORITHM THEORETICAL BASIS DOCUMENT

WIND VECTOR RETRIEVAL ALGORITHMS FOR OCEANSAT-2 SCATTEROMETER

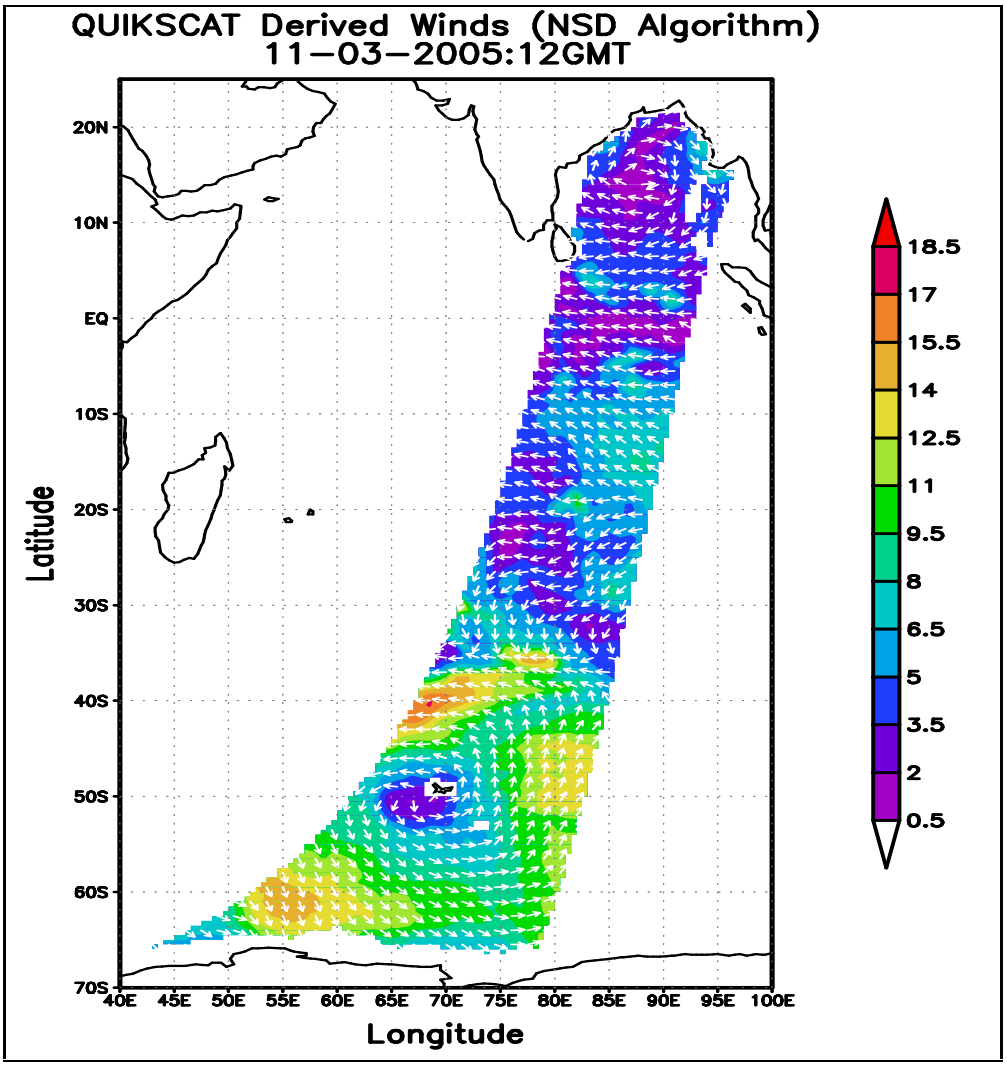

Space Applications Centre
Indian Space Research Organisation
Ahmedabad- 380015

June 2007

GOVERNMENT OF INDIA
INDIAN SPACE RESEARCH ORGANISATION
SPACE APPLICATIONS CENTRE
AHMEDABAD – 380 015

DOCUMENT CONTROL AND DATA SHEET

1	**Date**	June 15, 2007
2	**Title**	Algorithm Theoretical Basis Document (ATBD): Wind vector retrieval algorithms for Oceansat-2 Scatterometer
3	**Version**	1.0
4	**Document No.**	OCEANSAT-II-UP/SCATT-1/SAC-2007
5	**Type of Report**	Scientific
6	**No. of pages**	38
7	**Authors**	B.S. Gohil, K. Satheesan and A.K. Varma
8	**Originating Unit**	OSD/MOG/RESIPA, Space Applications Centre, Ahmedabad
9	**Abstract**	Oceansat-II, the second in the series of IRS satellites for oceanographic applications will carry a microwave Scatterometer (SCAT) and an advanced Ocean Colour Monitor (OCM). This document describes the various algorithms to be used for the retrieval of ocean surface wind vector from the OCEANSAT-II satellite scatterometer data. The document contains details of algorithms for extraction of wind vector solutions, wind directional ambiguity removal and flagging of rain and sea-ice. It also describes the procedures for post-launch development of geophysical model function (GMF) and rain impact model necessary for operational wind retrieval and rain flagging. Also described here are the simulation based studies using Quikscat GMF and rain impact models for wind vector retrieval, noise impact on retrieval and rain flagging.
10	**Classification**	General
11	**Circulation**	All concerned

SUMMARY

This Algorithm Theoretical Basis Document (ATBD) describes algorithms for retrieval of ocean surface wind vector from Oceansat-2 Scatterometer data. The ATBD contains three major algorithms for derivation of wind vector solutions, directional ambiguity removal and rain flagging. It also describes two crucial aspects specific to Oceansat-2, firstly, the development of Geophysical Model Functions (GMF) needed for wind vector retrieval and secondly, the development of rain impact model necessary for rain flagging. In order to realize retrieval as well as flagging, requirements of different types of global data sets are also specified along with its utilization procedures.

For deriving wind vector solutions, a new and efficient algorithm has been developed which is as good as Maximum Likelihood Estimator (MLE) algorithm being used operationally for the earlier and ongoing global scatterometer missions. The algorithm developed for directional ambiguity removal is based on median filter and it operates in two stages considering observational data at different spatial coverage in order to tackle the localized ambiguities also. The rain flagging algorithm makes use of the cost function developed for wind solution extraction which gets modified under rain free and rainy situations. The sea-ice flagging approach is adopted from the literature which is used for sea-ice detection from Quikscat data. The present ATBD describes the procedures for developing GMF specific to Oceansat-2 scatterometer by using simultaneous observations of radar backscatter from Oceansat-2 and reanalysis wind vector fields from AGCM (atmospheric general circulation model - ECMWF) for rain free conditions using rain information from TRMM or DMSP-SSM/I. Like-wise, procedures for rain impact model development are also described in ATBD based on atmospheric attenuation and rain fall to be available from TRMM-PR along with Oceansat-2 scatterometer radar backscatter and model analysis wind data.

Analysis of limited data of Quikscat scatterometer, sensitivity studies related to wind vector retrieval using both the algorithms (MLE and in-house), rain and sea ice flagging, assumptions made in algorithms and various procedures, and overall limitations of retrievals are also presented.

1.0 Introduction:

The ocean surface wind is the main driving force for ocean circulation and for generation of surface waves and currents. It plays an important role in air-sea interaction, upwelling, biogeochemical transport in the ocean and several other processes. The ocean surface wind vector is an essential input parameter for prediction models of ocean circulation and waves, which are used for oceanographic applications and climate related studies. It is also an indispensable parameter along with a few others, for the prediction of storm surges caused by storms formed in the oceans, which hit the coasts causing disaster in the coastal regions. Besides meteorological applications, ocean surface wind provides forcing parameters for studying the ocean general circulation. Scatterometer data can also be useful for ocean wave mapping and wave forecasting, offshore activities, ship routing, fisheries etc. Besides, wind vectors from scatterometer, when properly assimilated in an appropriate numerical model, helps improving weather forecast. Repetitive measurements of surface wind field over global oceans are thus necessary for the above studies and applications.

Wind vectors are usually obtained from microwave scatterometers operating at microwave frequencies in 5-14 GHz range. This part of the spectrum is useful for measurements under all weather conditions except heavy precipitation. However, the wind speeds can also be obtained from space-borne microwave radiometers and altimeters. Moreover, the upcoming microwave polarimetry is being considered for vector wind measurements.

2.0 Scatterometer measurements:

Active microwave remote sensing of ocean surface winds has started since the launch of SEASAT in 1978. This was the first satellite dedicated to the ocean research and was an experimental satellite, which demonstrated the retrieval of wind to an accuracy of 2 m/s, from wide swath scatterometer. ERS-1 & 2 satellites were launched with C-band microwave scatterometers. Japanese satellite ADEOS-1 carried a Ku-band scatterometer. Pencil-beam scatterometers operating at Ku-band were launched onboard ADEOS-2 and Quikscat satellites. Quikscat scatterometer is currently in orbit. A similar pencil-beam scatterometer operating at Ku band is due for launch onboard Indian satellite Oceansat-2 satellite.

Scatterometer is an active microwave instrument (radar), which measures the microwave energy backscattered from an area over the earth's surface illuminated by it. From the known transmitted and backscattered energy along with measurement geometry and other sensor related parameters, the radar backscatter coefficient or the normalized radar cross section (NRCS) symbolized as σ^0 (sigma naught) is derived. The σ^0 measurements over the ocean are used for wind vector determination. The philosophy of wind retrieval is discussed later, however, multiple measurements of backscatter are required for this purpose and scatterometers are designed to realize the same with multiple beams (antennae) in configurations like fan-beam or pencil-beam.

The fan-beam type employs two or more single or dual polarization antennae and has maximum azimuth separation of 90 degrees like those launched onboard Seasat, ERS-1/2 and ADEOS-1 satellites. The pencil beam type scatterometers observe radar backscatter at different azimuth separation angles like those launched onboard ADEOS-2 and Quikscat satellites. Retrieval of the surface wind vector in terms of speed and direction takes place using these so called 'triplets', 'quadruplets' or multiple of radar backscatter through a model known as Geophysical Model Function (GMF) which relates polarized backscatter with wind speed, wind direction and observational geometry.

3.0 Oceansat-2 scatterometer system:

Oceansat-2 satellite in sun-synchronous orbit at 720 km altitude will carry a Ku-band microwave scatterometer (SCAT) and an Ocean Colour Monitor (OCM). The satellite will have two days repeat cycle with equator descending time around noon.

The scatterometer system has a 1-m parabolic dish antenna and a dual feed assembly to generate the two beams and is scanned at a rate of 20.5 rpm to cover the entire swath. The inner beam makes an incidence angle of ~ 49° and the outer beam makes an incidence angle of ~ 57° on the ground. It covers a continuous swath of 1400 Km for inner beam and 1840 Km for outer beam respectively. The inner beam is configured in horizontal polarization and the outer beam is configured to vertical polarization for both transmit and receive modes. The horizontal polarization is chosen for inner beam in order to alleviate the low backscatter value problem of horizontal polarization at lower wind speeds. This would ensure the reduction in the path loss due to the slant range and hence maintains an almost the same SNR for both the inner and outer

beams. Brief specifications of the scatterometer view geometry are provided in Table (1). Figure (1a) shows the viewing geometry of the scatterometer (SAC, 2005).

Table 1: Technical characteristics of Oceansat-2 Scatterometer

Parameters	**Inner Beam**	**Outer Beam**
Altitude	720 Km	
Look Angle	42.62°	49.38°
Incidence Angle	48.9°	57.6°
Swath	1400 Km	1840 Km
One way 3-dB Beam Width	1.47° x 1.67°	1.47° x 1.67°
One way 3-dB foot Print	26 Km X 46 Km	31 Km X 65 Km
Nominal Slice Width (Across Scan)	8Km	8Km
Inter center spacing along Track	19 Km	19 Km
Inter center spacing along scan	15 Km	19 Km

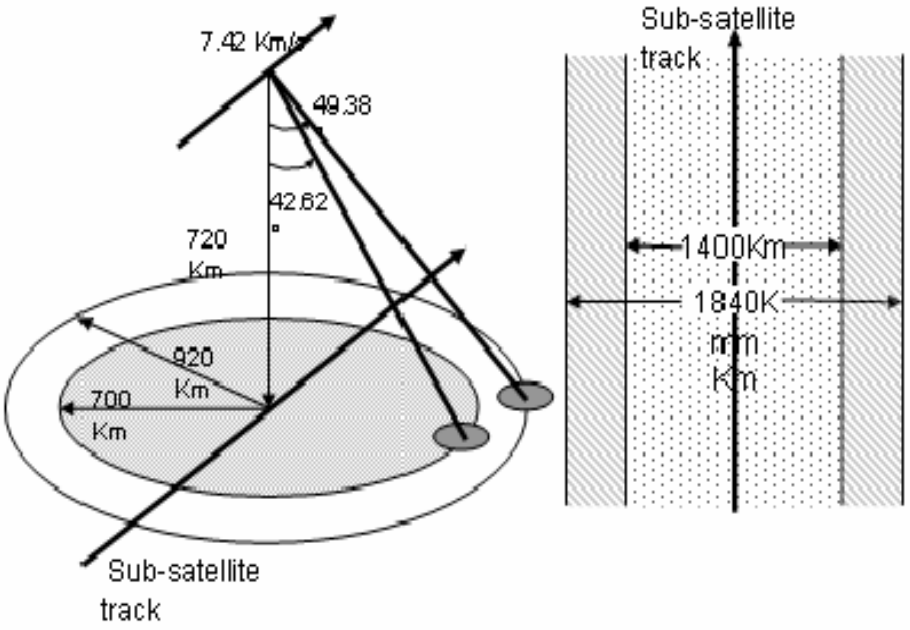

Figure 1a: Viewing geometry of Oceansat-2 Scatterometer

3.1 Oceansat-2 scatterometer data swath:

Various types of the wind vector cells available from a pencil-beam scatterometer are depicted in figure (1b). Due to circular scanning of two beams at fixed incidence angles, areas of a particular size cut across the swath contain variable number of backscatter measurements impacting the wind retrieval. The entire swath can be divided

into three zones namely exclusive outer beam zone referred as outer zone, sweet zone and nadir zone.

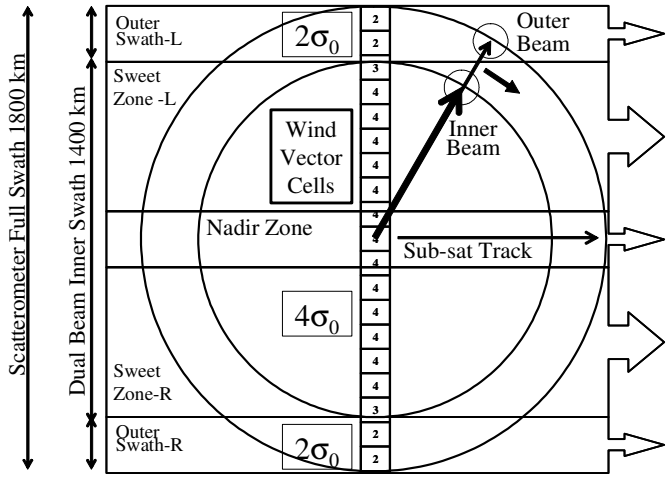

Figure 1b: Definition of wind vector cells and retrieval zones

Over outer zone, where no measurements from inner beam are available and the derived wind solutions do not posses any ranking, the wind retrieval needs external data like model winds. Over sweet zone, measurements available from both the beams with dual look directions also having good optimal azimuth diversity are very much suitable for better wind vector retrieval. Over nadir zone, measurements available from both the beams with dual look directions but with non-optimal azimuth diversity lead to more erroneous wind vectors. Wind direction ambiguity removal processes for outer and nadir zones are different and require special efforts mentioned briefly later.

3.2 Geophysical products specifications:

Given below are specifications as per the existing satellite mission, however, based on Oceansat-2 design, post-launch performance and GMF characteristics, these specifications may slightly deviate.

Table 2: Geophysical product requirements:

Geophysical Parameter	***Range**	***Accuracy (rms)**
Wind Speed	3 – 20 m/s 20 – 30 m/s	2 m/s 10 %
Wind Direction	0 – 360 Deg.	20
*At 25 km wind vector cell (NASA, 2006), Minor deviation anticipated for Oceansat-2		

3.3 Oceansat-2 scatterometer data processing flow:

Figure (2) depicts the process flow from Level 2A scatterometer data product to the Level 2B wind vector data product including flags. It consists of two primary inputs namely radar backscatter with ancillary information and the model wind forecast. The use of retrieval module with its various components and other modules are depicted.

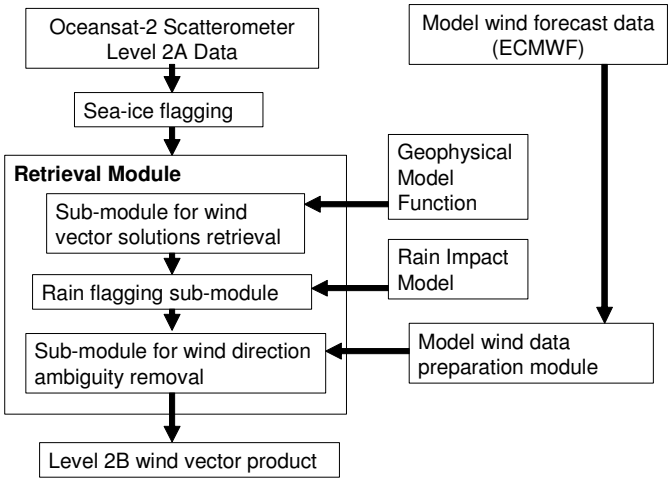

Figure 2: Process flow for various types of data products

4.0 Geophysical model functions:

The magnitude of radar backscatter depends upon the sea surface roughness generated by the action of winds. The wind forcing generates a spectrum of surface waves in which growth of capillary waves is directly influenced by wind intensity. The basic mechanism at work is the Bragg Resonance, in which the waves satisfying Bragg's condition produce strong radar backscatter energy. The backscatter signal also depends upon the incidence angle of radar beam. The directional anisotropy of the radar signal, caused by the azimuth symmetry of sea surface roughness, yields multiple solutions of derived wind vectors (especially direction). Among these, only one solution is "true" and remaining solutions are known as directional "ambiguities". Multi-beam scatterometer is used to overcome this problem of ambiguities to a certain extent. The radar backscatter shows a harmonic nature as expressed by (Ulaby et al, 1981, Wentz and Smith, 1999 and others)

$\sigma^0(W, \varphi, p, \theta) = \sum_{i=0}^{Nh} B_i.\cos(i.\varphi)$ with $B_i = P_i(p,\theta).W^{Q_i(p,\theta)}$	1

where, φ is relative wind direction ($\varphi = \chi - \phi$), an angle between radar azimuth ϕ and wind direction χ both measured in meteorological convention (clockwise from local North direction with a zero degree wind direction representing a wind blowing from North to the point of observation). Here, the ocean surface wind speed W is at neutral stability height of 10 m. The coefficients B_i are harmonic components with P_i and Q_i coefficients expressed as functions of polarization p and incidence angle θ at a given radar operating frequency and Nh is the number of harmonics considered. As, so far, the observed dependency of radar backscatter on wind conditions has not been well-explained theoretically, the empirical relationships are established using simultaneous measurements of radar backscatter and ocean surface wind vector obtained through model analysis as well as insitu measurements. The Geophysical Model Function (GMF) is an empirical relationship between radar backscatter and wind vector.

In equation (1), the non harmonic component (or the constant term) signifies the base value of variation of radar backscatter for a given wind speed, incidence angle and polarization, the first harmonic represents the upwind-downwind ratio of backscatter while second harmonic which is dominant among all other harmonics signifies the upwind-crosswind ratio. Though the third harmonic representing the skewness around cross wind direction is very small in value but along with the first harmonic, it is very important for the wind direction retrieval.

4.1 Prevailing GMF:

There are various GMFs available for Ku-band known as SASS-1, SASS-2, NSCAT-1, NSCAT-2, and QSCAT-1. The functional forms of these GMFs are given by Schroeder et al, (1982); Wentz, (1994); Wentz and Smith (1999) and Dunbar (1999). As an example of the difference among GMFs, the variation of horizontal polarization radar backscatter from NSCAT-1 and QSCAT-1 GMFs at different wind speeds is depicted in figure (3).

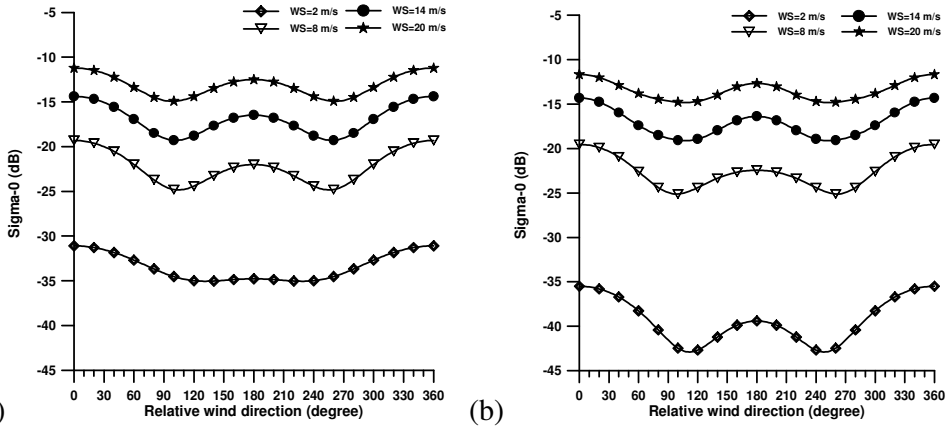

Figure 3: Variation of horizontally polarized σ^0 with relative wind direction at incidence angle of 46 degree using different GMFs, (a) NSCAT-1, (b) QSCAT-1

It is important to note that these GMFs are system specific and vary from system to system. Hence, these GMFs are required to be redeveloped or refined for an independently designed scatterometer system.

4.2 GMF development procedures:

After normalization with the constant term, the equation (1), considering variations in radar backscatter up to third harmonic of wind direction, is rewritten as

$\sigma^0 = A_0[1+A_1.\cos(\varphi)+ A_2.\cos(2\varphi)+ A_3.\cos(3\varphi)]$	1a

where, the coefficients A_i are functions of wind speed, incidence angle and polarization. In order to determine the coefficient A_0 at desired incidence angle, wind speed and polarization, the σ^0 values for all relative wind direction φ varying from 0 to 2π are averaged yielding A_0 coefficient as the summation of $\cos(\varphi)$, $\cos(2\varphi)$ and $\cos(3\varphi)$ vanishes

$A_0 = \langle\sigma^0\rangle$	2

Dividing equation (1a) by A_0 on both sides and rearranging the terms we get

$Y = A_1 \text{Cos}(\varphi) + A_2 \text{Cos}(2\varphi) + A_3 \text{Cos}(3\varphi)$ where $Y = (\sigma^0/A_0) - 1$	3

At desired incidence angle, polarization and wind speed, by determining Y at each φ value, the harmonic coefficients A_i are established through statistical analysis. This procedure yields the GMF coefficients as well as an idea about the scatterometer data quality.

It is important that for each bin of wind speed the wind direction corresponding to radar backscatter should have uniform distribution with statistical significance while for any bin of relative wind direction the wind speed should have Rayleigh distribution (Wentz et al, 1984). Thus, it requires a large database of simultaneous backscatter and wind vector measurements in order to meet this requirement for GMF development. Moreover, the data should also be for rain free situations requiring simultaneous observations of rain.

As a prelude to GMF development, analysis of Quikscat data (MGDR NRT Version in BUFR format at 25 km spatial resolution) for orbit #29820 on March 11, 2005 at 12.00 GMT is performed. Figure (4) shows the scatter plot of Quikscat radar backscatter with relative wind direction obtained making use of NCEP model winds provided along with the data.

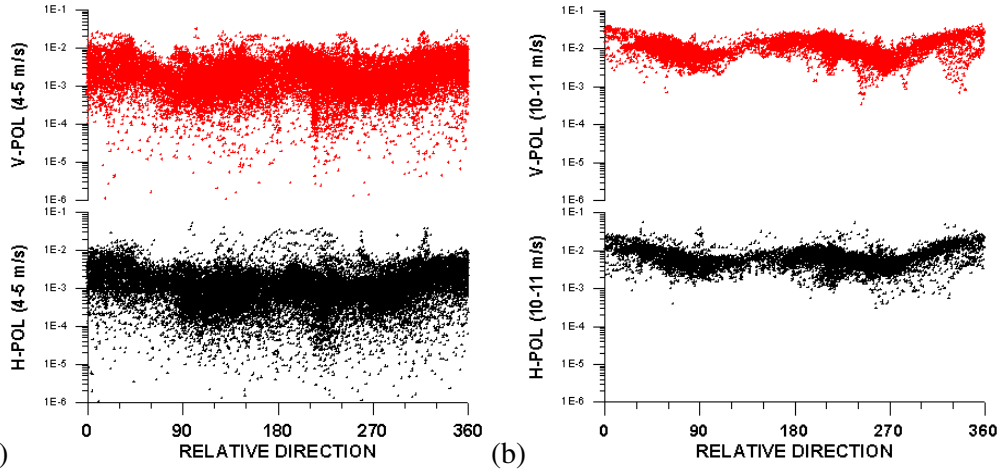

(a) (b)

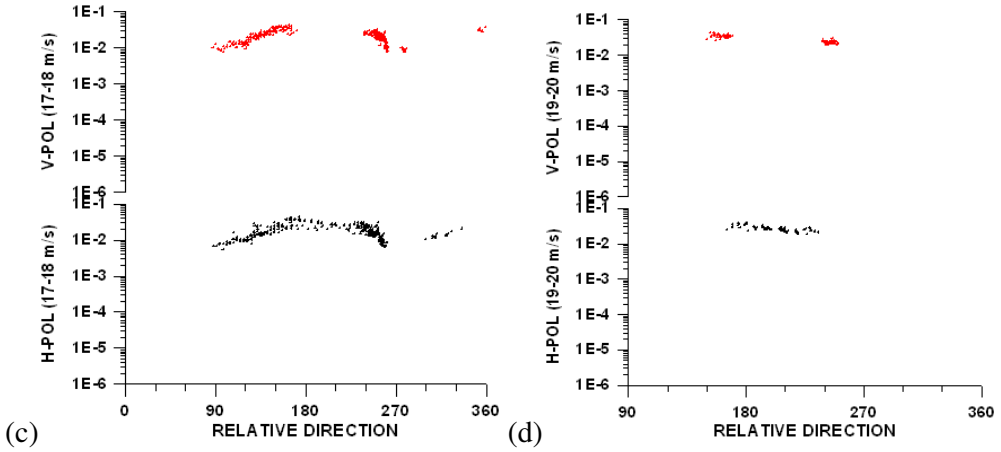

Figure 4: Distribution of horizontal and vertical polarization radar backscatter with relative direction for one orbit of Quikcat scatterometer for various wind speed bins at, (a) 4-6 m/s, (b) 10-11 m/s, (c) 17-18 m/s and (d) 19-20 m/s.

The A_0 coefficients for selected wind speed values are derived from the above Quikscat data as depicted in figure (5). A comparison of derived A_0 from the data set and from the Quikscat GMF QSCAT-1 is also depicted. The observed difference between GMF and data derived A_0 coefficient is quite evident due to incompleteness of the observation set.

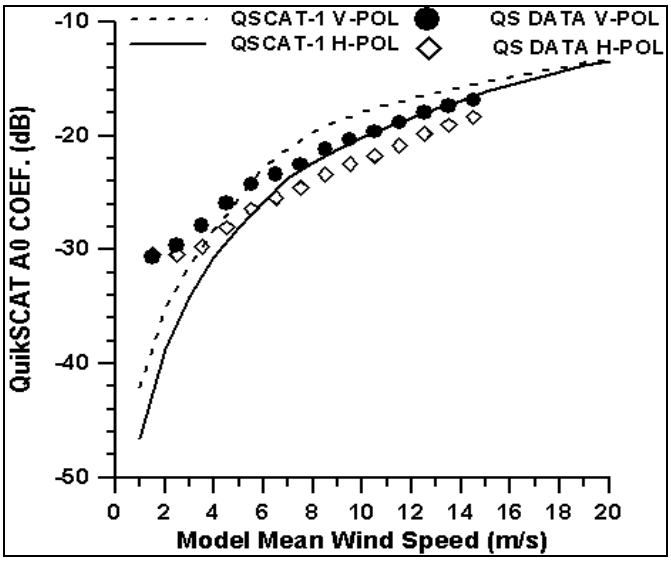

Figure 5: Comparison of A_0 coefficients derived from Quikscat data and the QSCAT-1 GMF.

Due to the non-availability of large data sets of radar backscatter, the above exercise with radar backscatter simulated using NSCAT-1 and QSCAT-1 GMFs has been performed for wind speed only up to 20 m/s which is the specified range for NSCAT-1. The comparison of harmonic coefficients (proxy GMF) established using these two GMFs has been performed (Tiwari and Gohil, 2005) as shown in figure (6). The difference in two GMFs in terms of harmonic coefficients is quite evident. Moreover, the NSCAT-1 and QSCAT-1 GMFs were developed considering two and three harmonics, respectively. The comparison reveals the fact that the GMFs are sensor specific.

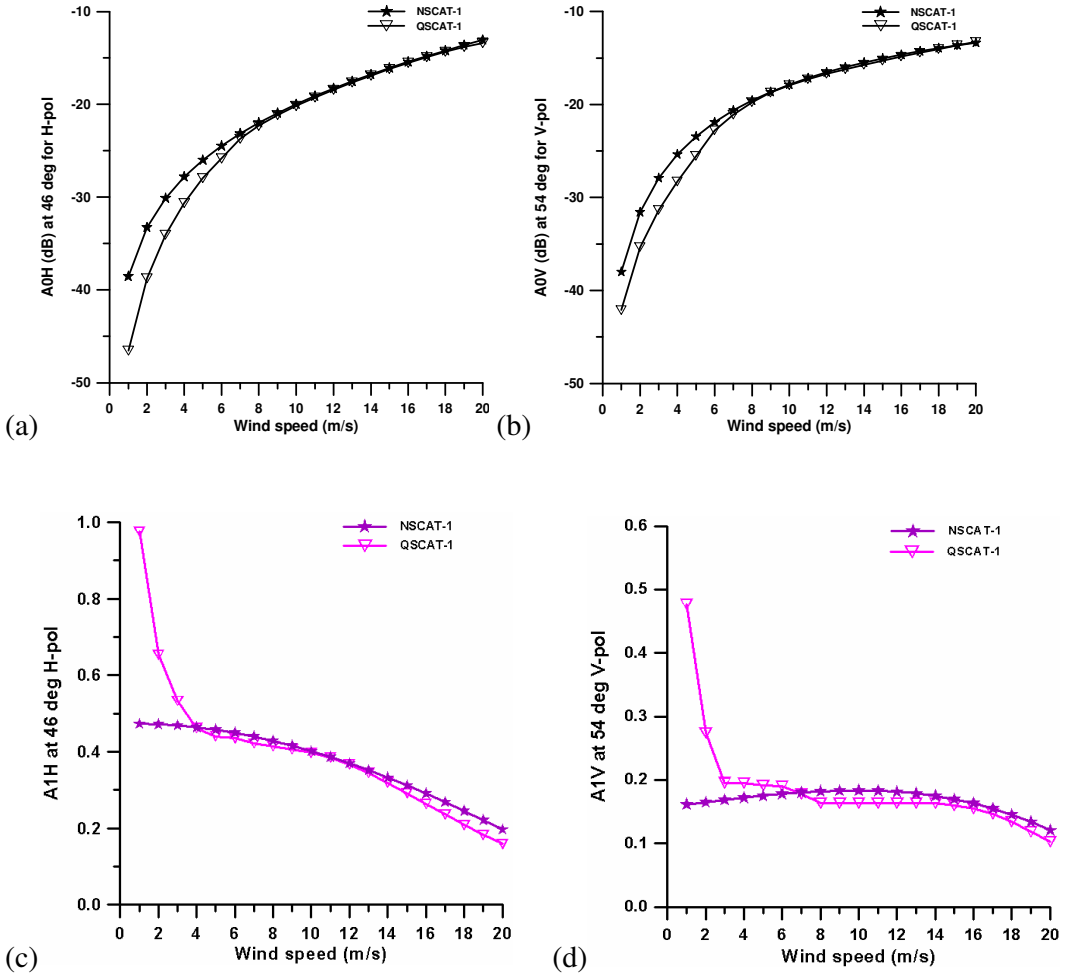

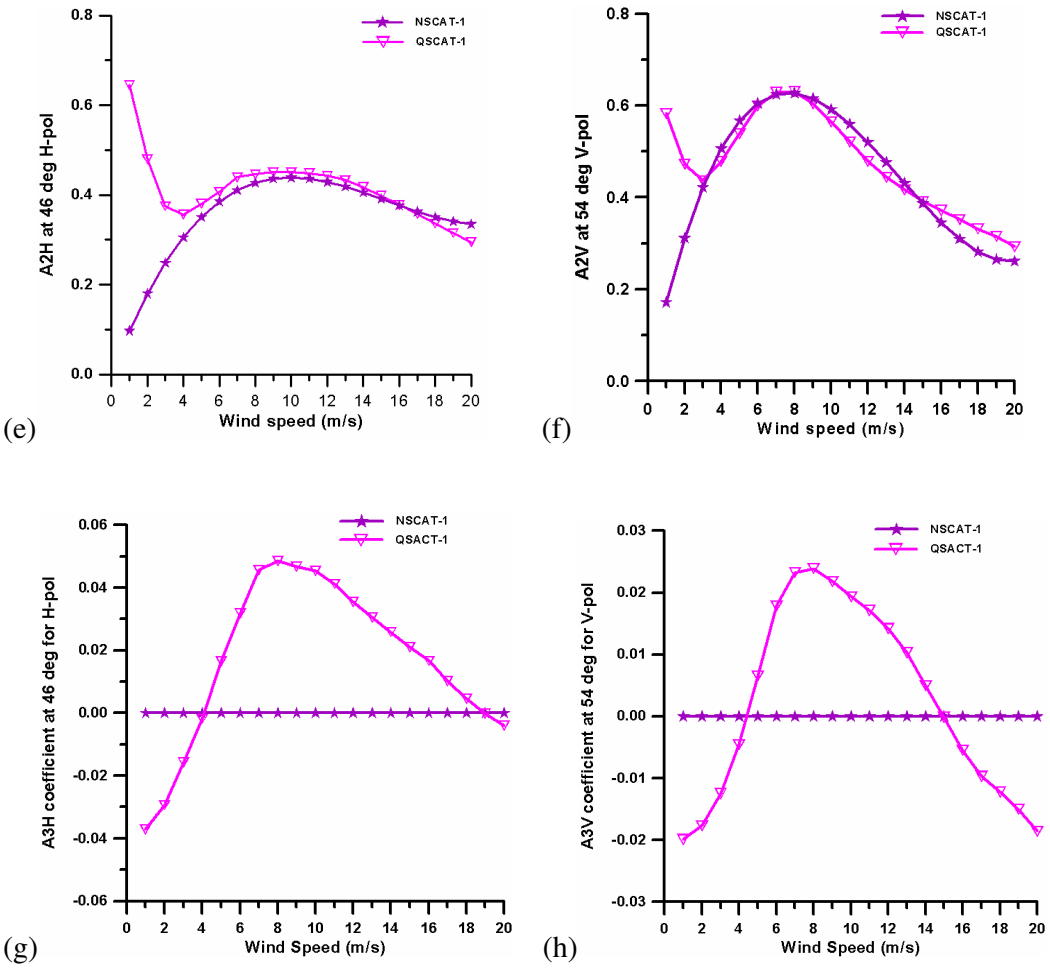

Figure 6: Comparison of harmonic coefficients established using NSCAT-1 and QSCAT-1 GMFs

4.2.1 Post-launch ancillary data requirements for GMF development:

The basic data sets needed are the global observations of radar backscatter from Oceansat-2 scatterometer and near concurrent model analysis wind vector data. In order to develop GMF for rain free conditions, near concurrent observations of rain is also required from other satellites like TRMM-PR/TMI and DMSP-SSM-I. The collection of these data sets is planned for about six months from the launch of Oceansat-2 satellite. The justification for six month period is that a sufficient data base is required to be prepared to cover the widest range of wind speed as well as the entire range of wind direction for all wind speed preferably the low and high speed ranges also pertaining to rain free situations. The data required for GMF development is reflected in Table (3).

Table 3: Ancillary data for Oceansat-2 scatterometer GMF development:

Source	Sensor	Parameter
Satellite	Oceansat-2/ Scatterometer	Backscatter & ancil. data
	TRMM-PR/TMI and SSM-I	Rain rate
Global Models	ECMWF/ NCEP/ NCMRWF Model analysis	Wind speed and dir, SST, surface air temp. and humidity
Insitu	NIOT/ NIO/ -ICOADS /TRITON buoys, AWS and ship cruise data	Wind speed and dir

5.0 Wind vector retrieval and the state of art:

The radar backscatter having harmonic dependence on wind direction yields multiple solutions of wind vector from a given set of radar backscatter measurements. As the radar backscatter is a function of wind speed and direction, two measurements of radar backscatter are essentially required to determine wind vector. However, unique solutions are not possible due to the harmonic nature of backscatter on wind direction and the presence of noise in radar data. Among these multiple wind vector solutions, only one solution corresponds to true wind vector while others are ambiguities also known as "aliases". Although, the wind speed solutions are very close to each other, the direction solutions are quite apart. The solutions are prioritized (or ranked) based on certain criterion used in algorithm. The performance of the algorithm is evaluated in terms of percentage of highest priority (rank-1) solutions correctly identifying the true directions out of the total number of data cases processed.

Under noise-free conditions, the rank-1 solution always represents the true wind vector but for noisy or real data, it is always not so. However, the first two highest ranked solutions contain the true direction most of the times. The selection of vector solution nearest to the true wind vector is performed through the directional ambiguity removal algorithm. An overall scheme for retrieval of wind vector field is depicted in figure (7).

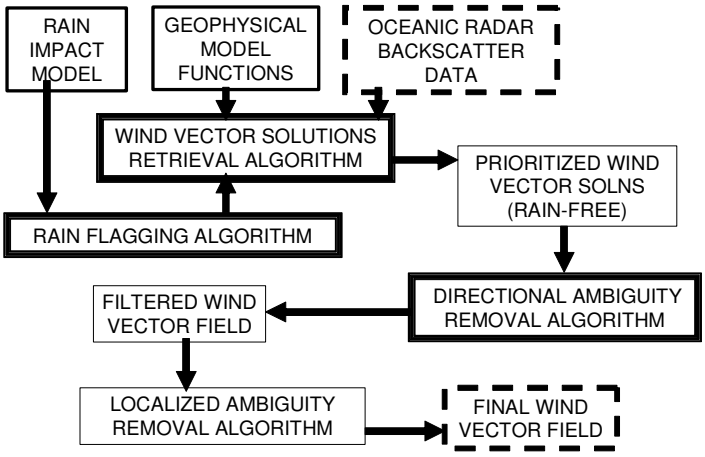

Figure 7: An overall scheme for retrieval of wind vector field

5.1 Algorithm for retrieval of wind vector solutions:

The maximum likelihood estimator (MLE) algorithm developed based on Bayesian approach is the best algorithm (Chi and Li, 1988), which is widely and operationally used for the scatterometer missions launched so far. More so, variants of MLE algorithm have also been developed (Stoffelen and Anderson, 1997; Stoffelen and Portabella, 2006) with difference in its implementation. In some of the variants of MLE, a transformed MLE has also been developed. The algorithm developed recently is based on transformed MLE, which is as good as MLE but is computationally efficient. This recently developed algorithm is described here. The cost function used in MLE algorithm (Pierson, 1989), is given as

$$MLCF(W_k, \chi_k) = \Sigma_{i=1}^{M} \{(\sigma^{0M}(\phi_i, \theta_i, p_i) - \sigma^{0G}(W_j, \varphi_{ki}, \theta_i, p_i)) / Kp_{ij}.\sigma^{0G}(W_j, \varphi_{ki}, \theta_i, p_i)\}^2 \quad (4)$$

Where, σ^{0M} is backscatter measured by i^{th} scatterometer antenna beam at incidence angle θ_i, polarization p_i with azimuth direction ϕ_i, σ^{0G} is backscatter calculated from GMF for a trial wind speed Wj and trial k^{th} wind direction χ_k, φ_{ki} is relative wind direction taken as $\varphi_{ki} = \chi_k - \phi_i$ and ϕ_i is antenna azimuth direction from North direction.

For an assumed wind direction, the cost function MLCF is minimized by using simulated backscatter for varying wind speed W_j with a suitable increment and the

nonlinear interpolation. The minimum of MLCF is dependent on the wind speed search interval. As smallest is the interval (more computations) precise is the minimum. This process can also be realized using individual minimization for which the MLCF is transformed from backscatter space to the wind speed space and is referred here as normalized variance (NV) given by

$$NV_k = \sum_{i=1}^{M} \{(W_{ki} - W_k) / Kp_i W_k\}^2 \quad (5)$$

Where W_{ki} is a wind speed derived from i^{th} measurement $\sigma^{0M}(\phi_i, \theta_i, p_i)$ while W_k is a best (but with errors) wind speed to which all measurements are associated with.

In this recent approach, a given backscatter observation $\sigma^{0M}(\phi_i, \theta_i, p_i)$ is converted into wind speed W_{ki} for an assumed wind direction through GMF as

$$W_{ki} = W_j \quad \text{such that} \quad \sigma^{0M}(\phi_i, \theta_i, p_i) = \sigma^{0G}(W_j, \varphi_{ki}, \theta_i, p_i) \quad (6)$$

Here, W_j is varied over the range specified by GMF being used and W_{ki} is obtained numerically through linear interpolation of σ^{0G} and W_j (due to its closure form and hence efficient).

The derived wind speed W_{ki} is a sum of true speed W_{Tk} and an error W_{Eki} which is a manifestation of errors in backscatter. The true error in σ^{0M} is unknown but is represented by variance of σ^{0M} (communication noise) defined in terms of Kp value which can be calculated using model backscatter (GMF) and the sensor parameters α, β and γ (Fischer, 1972; Long and Mendel, 1991; Oliphant and Long, 1999) as

$$Kp_i = \sqrt{((\gamma_i / \sigma^{0G}{}_i^{\,2}) + (\beta_i / \sigma^{0G}{}_i) + \alpha_i\ }} \quad (7)$$

Thus assuming $W_{Eki} = Kp_i.W_{Tk}$, the W_{ki} can be redefined considering the backscatter variance as

$$W_{ki} = W_{Tk}(1 + Kp_i) \quad (8)$$

Using M number of σ^{0M} measurements, the backscatter variance-weighted mean of derived wind speed for trial wind direction χ_K is defined as

$$W_k = \sum_{i=1}^{M} \{W_{ki} / (1+Kp_i)\} / \sum_{i=1}^{M} \{1 / (1+Kp_i)\} \quad (9)$$

Since W_{ki} is calculated assuming $\sigma^{0G} = \sigma^{0M}$, the Kp_i value cannot be calculated from σ^{0M}. For this reason, all Kp_i values are first initialized to zero, and then W_{ki} and corresponding Kp_i are calculated through GMF using equations (4) and (2), respectively. The W_k is recalculated using the updated values of Kp_i, and the procedure is repeated till W_k is converged yielding final Kp_i and W_k.

Since Kp value is already used in W_k, ignoring Kp in equation (5) yields NV as

$$NV_k = \sum_{i=1}^{M} \{(W_{ki} - W_k) / W_k\}^2 \quad (10)$$

The above term can also be expressed as normalized standard deviation (NSD) and standard deviation (SD) of wind speed derived from backscatter measurements as given below

$$NSD_k = (1/W_k)\sqrt{[(1/M) \sum_{i=1}^{M} (W_{ki} - W_k)^2]} \quad (11)$$

$$SD_k = \sqrt{[(1/M) \sum_{i=1}^{M} (W_{ki} - W_k)^2]} \quad (12)$$

The present algorithm referred as NSDA makes use of parameter NSD for deriving as well as for ranking the wind vector solutions. As NSD or SD are obtained from W_{ki} values which are derivable due to their closure form for a given trial direction, this approach becomes very efficient (Chi and Li, 1988). Based on SD without considering the measurement variance, an algorithm developed in-house was used for

SEASAT-A and ERS-1 scatterometers (Gohil and Pandey, 1985; Gohil, 1992; Gohil and Pandey, 1995). Retrieval algorithm using NSD ignoring Kp value was developed and tested with Quikscat data (Gohil et al, 2006). In the present study, NSD considering the Kp value is used for ranking the solutions. The parameter SD is used for rain flagging discussed later. A block diagram of algorithm for retrieving wind vector solutions is given in figure (8).

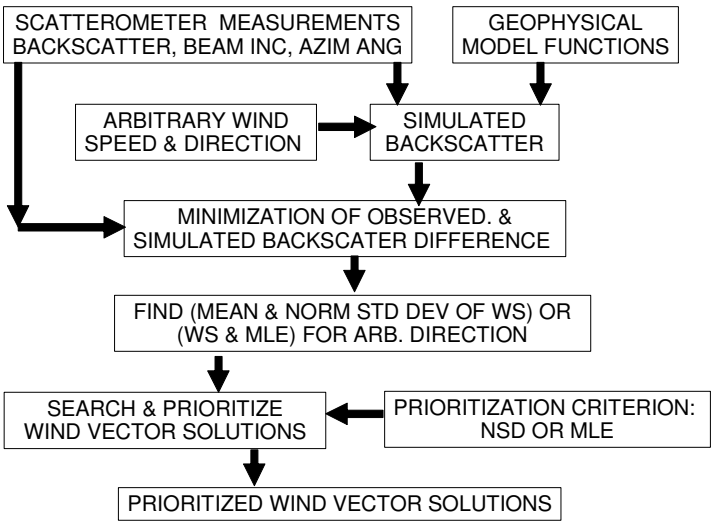

Figure 8: Block diagram of algorithm for retrieving wind vector solutions

5.1.1 Implementation of retrieval algorithms:

The NSDA is implemented in following steps:

1) First, assume $\delta\chi$ as 2°. For χ=0°, calculate wind speed WS_{1i} using equation (6) for the "i^{th}" backscatter measurement by varying wind speed over full GMF range with interval δ_{WS1} (1.0 m/s). Using all WS_{1i}, also find the weighted mean W_m and the normalized standard deviation NSD values from equations (9) and (11), respectively,

2) Truncating WS_{1i} with 1.0 m/s precision denoted by WS_{trnci}, evaluate wind speed regimes ΔWS_{1i} separately for all the beams using the following equation

$\Delta WS_{1i} = WS_{trnci} \pm \delta_{WS1}.\delta\chi$	13

3) Repeat steps (1 and 2) using ΔWS_{1i} for the remaining trial directions

4) Find vector solutions by searching minima of NSD along χ yielding N_S solutions with W^n_m wind speed and χ^n direction and the corresponding NSD^n values

5) Find precision direction solution χ^n_{prcn} through calculating minimum of quadratic fit of NSD^n values obtained for χ varied between $\chi^n \pm \delta\chi$ with 1° trial direction interval starting with wind speed search regime ΔWS_{1i} at $\chi^n - \delta\chi$ trial direction

6) At precision direction solutions χ^n_{prcn}, find W^n_m and NSD^n through step 2 exploiting ΔWS_{1i} values at $\chi^n - \delta\chi$ trial direction. The derived precision solutions of wind speed, direction and corresponding NSD are denoted by W^n_{mprcn}, χ^n_{prcn} and NSD^n_{prcn}, respectively

7) Rank the wind vector solutions on the basis of NSD values. The wind vector solution having minimum NSD is ranked as rank-1 solution and so on.

For comparison purpose, the MLE algorithm is also implemented in following steps:

1) First, assume a trial wind direction interval of 2°, denoted by $\delta\chi$. For χ=0°, find wind speed denoted by WS_1 corresponding to minimum MLCF determined as per equation (4) using wind speed varied over full GMF range with 1.0 m/s interval denoted by δ_{WS1}.

2) Evaluate wind speed regime ΔWS_1 from WS_1 using the following equation.

$\Delta WS_1 = WS_1 \pm 2\delta_{WS1}.\ \delta\chi$	14

3) Find wind speed denoted by WS_2 through searching MLCF minimum using wind speed regime $\Delta WS_1$with 0.2 m/s wind speed interval termed as δ_{WS2}.

4) Find precision wind speed WS_{2prcn} through minimum of quadratic fit of MLCF around WS_2 with winds between $WS_2 \pm \delta_{WS2}$ and recalculate $MLCF_{2prcn}$ for WS_{2prcn} at χ=0°.

5) Truncate WS_{2prcn} with 0.2 m/s precision denoted by WS_{trnc} and find the wind speed regime for the next trial direction χ is given as

$\Delta WS_2 = WS_{trnc} \pm 2\delta_{WS2}.\ \delta\chi$	15

6) Repeat steps (3 through 5) for the remaining trial directions varied with an interval $\delta\chi$ with wind corresponding to wind speed regimes given by equation (14).

7) Find vector solutions by searching minima of $MLCF_{2prcn}$ along trial direction. Denote number of solutions as N_S and their serial numbers as n. The solutions of wind speed, direction and the corresponding MLCF thus obtained are denoted by WS^n, χ^n and $MLCF^n$, respectively, where n varies from 1 to N_S.

8) Find precision direction solution χ^n_{prcn} around χ^n by finding minimum of $MLCF_{2prcn}$ through quadratic fit of $MLCF_{2prcn}$ values calculated for χ varied between χ^n and $\chi^n \pm 3\delta\chi$ with 1° direction interval.

9) Find WS^n_{prcn} and $MLCF^n_{prcn}$ at the precision direction solution χ^n_{prcn} following steps (3 through 5) exploiting the wind speed regime of $(\chi^n - \delta\chi)^{th}$ trial direction.

10) Repeat step 9 for all N_S solutions.

11) Rank wind vector solutions on the basis of MLCF values. The wind vector solution having minimum MLCF is ranked as rank-1 solution and so on.

In step 8 for MLE and steps 5 and 6 for NSD implementations, the continuity of the trial direction (circular data) and associated parameters around upwind direction is maintained. The above schemes are found to be effective in finding precise solutions not only for maintaining the direction retrieval skill of the algorithm under varying $\delta\chi$ (finer to coarser) and for minimizing the artifacts of search intervals and quadratic fitting but also for enhancing the computational efficiency. The typical values of search intervals mentioned above are optimized based on the noise free cases considering the entire inner beam swath including nadir region. The litmus test for proper implementation of the algorithm is that the retrieval skill for the noise free cases must be 100%. The condition shown by expression (13) is effective in the situations when coarser search intervals of trial direction are used. However, the coarser $\delta\chi$ should be avoided due to possibility of missing proper solutions specifically over the nadir region and the retrieval becomes less computationally efficient. Moreover, δ_{WS2} also cannot be increased in order to retain the accuracy of quadratic interpolation. The optimization of search interval, to some extent, also depends upon the intervals of wind speed and direction specified in GMF. The values of search intervals $\delta\chi$ and δ_{WS1} mentioned above are optimized based on the QSCAT-1 GMF.

Based on simulations, primarily the evaluation of performances of the proposed algorithm in successfully retrieving the wind direction under varying noise conditions has been carried out for the inner beam data swath region including nadir region. In order to carry out simulation studies, radar backscatter data for Quikscat scatterometer observational geometry is simulated with orbital altitude of 803 km and local incidence angles of 46° and 54° at the earth's surface with horizontal and vertical polarization, respectively. The outer beam swath is divided in a number of wind vector cells (WVC), and for each cell, azimuth angle with respect to sub-satellite track is calculated for each of the antenna beams pointing to the cell. The cells with only four beams are used for the simulation studies. At these WVC, radar backscatter data are simulated using QSCAT-1 geophysical model function (rsd@zephyr2.jpl.nasa.gov) for simulated wind vector with wind speed and direction values varied within the specifications of QSCAT-1 GMF. The details of QSCAT-1 GMF are available online (Dunbar, 1999). The GMF backscatter value for any relative wind vector and incidence angle within GMF specifications can be obtained through bi-linear interpolation. The modification of simulated backscatter due to rain is realized through the rain model (Draper and Long, 2004) yielding the path integrated attenuation PIA and the lump rain backscatter contribution σ^0_{rw} as functions of integrated rain rate R expressed in km.mm/hr as

$\sigma^0_r = e^{-PIA}.\sigma^0_g + \sigma^0_{rw}$	16

Based on Quikscat data (25 km BUFR Format) for one orbit, the most prevalent values of α, β and γ with their respective standard deviations are used for simulating noisy backscatter data for testing the algorithms. These parameters, in general, are expressed here as

$Y(j) = Y_m + V(j)$	17

where Y may be α, β or γ, with Y_m as respective mean representative value. The Gausian random variable V(j) has zero mean and standard deviation as observed in Quikscat data given in table (4).

Table 4: Kp parameters of Quikscat data

Kp Parameter (Y)	Y_m	V
α **(kp_alpha-1)**	$1.0.10^{-2}$	$0.3.10^{-2}$
β	$1.0.10^{-5}$	$0.3.10^{-5}$
γ	$1.0.10^{-7}$	$0.3.10^{-7}$

For each case of wind vector cell, wind vector and antenna beam, the values of α, β and γ are generated to simulate the noisy backscatter (Oliphant and Long, 1999) as

$$\sigma^{0M}i = \sigma^{0G}_i (1+Kp_i.X_i) \quad (18)$$

where X_i is another independent Gausian random number with zero mean and the standard deviation K. The value of standard deviation K is normally unity, however, it can be varied for controlling the noise in simulation experiment. For noise free case, the value of K is zero and for noisy cases, it is varied from 1.0 to 2.0. The Kp is given by equation (7). While studying the impact of rain on wind vector retrieval, the rain model is used only for simulating the noisy backscatter data but not for the retrieval purpose.

5.1.2 Characteristics of wind retrieval across the inner beam swath:

The simulation experiment carried out for noise free cases provides an insight into the characteristics of wind solutions at different locations of the swath. Over the sweet zone (Figure 9a) due to the optimum azimuth separation the sensitivity of cost function (NSD) with respect to aspect direction is higher. This leads to the retrieval skill relatively higher as compared to the other regions due to optimum azimuth separation as well as dual polarized multi-look measurements. Over near nadir region, despite dual polarization multi-look measurements, the azimuth separation is non-optimal leading to lower sensitivity of cost functions as seen in figure (9b) leading to reduced retrieval skill and higher errors. At the sub-satellite track, the retrieval skill is approximately halved due to

pairing of solutions in terms of ranking criterion as seen in figure (9c). The retrieval errors are also more due to non-optimal azimuth separation.

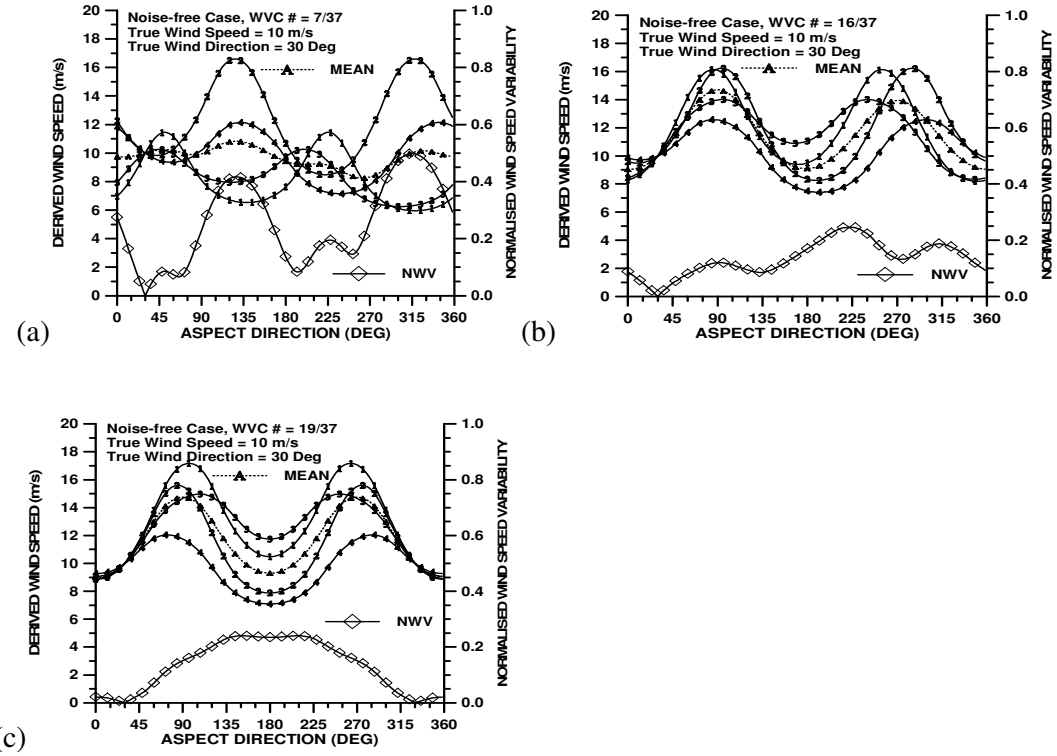

Figure 9: Characteristics of wind solutions across the inner beam swath over, (a) Sweet zone, (b) near nadir zone, (c) sub-satellite location

5.1.3 Comparison of retrieval algorithms and the noise sensitivity:

The retrieval performance (or skill) of an algorithm for a particularly ranked (first, second, etc) solution is defined in terms of percentage of total number of simulated wind vectors bearing that particular rank are closest to the wind directions used in simulating the radar backscatter data through GMF. Algorithm implementation is verified by observing 100 percent skill of top ranked solutions for noise-free condition (K=0) also with even and odd intervals of trial direction for retrievals as well as for simulating backscatter data. For MLE algorithm a small GMF modeling error (1.0e-14) is used to avoid division by zero in MLCF calculations. For the swath location exactly at the sub-satellite track where azimuth separation is 180, the skill is 50% irrespective of the algorithm as pairing of solutions takes place with the same ranking.

The performances of MLE and NSD algorithms are evaluated for K=1.5 as depicted in figure (10a). The skill is evaluated separately for each wind vector cell (WVC) location numbered from 1 to 37 across the swath. The WVC numbered 19 corresponds to the sub-satellite track position. The algorithm skill for each WVC is evaluated using wind vector cases with wind speed varying from 1 to 25 m/s with 2 m/s interval and wind direction varying from 0° to 354° with 6° interval yielding total 780 data points. The backscatter data are perturbed with noise controlled by parameter K with GMF modeling error of 1.0e-14. It is also observed from figure (10a) for K=1.5 that MLE and NSD algorithms have almost equal performances. The retrieval errors in wind speed and direction of both the algorithms as shown are found to be almost comparable. Apart from this, comparison of distribution of directions retrieved using these algorithms is also performed as shown in figure (10b) and is also found to be mostly similar.

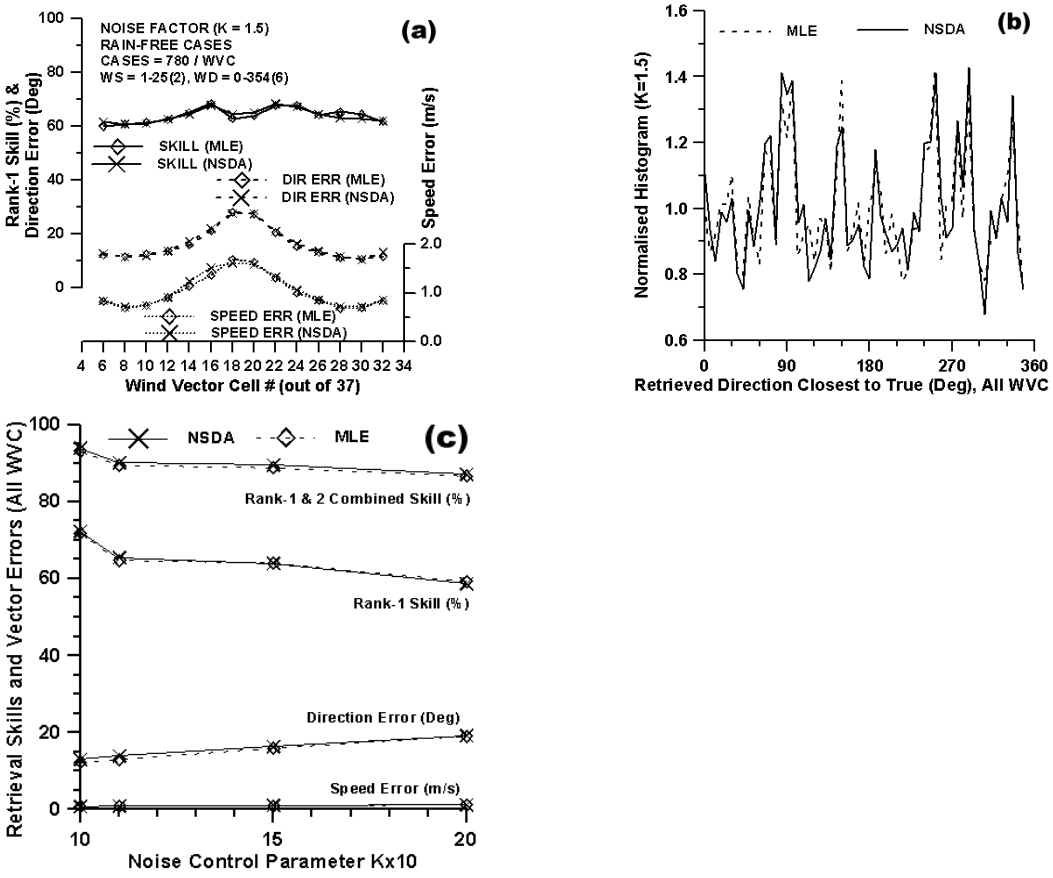

Figure 10: Characteristics of MLE and NSD algorithms, a) Comparison of direction retrieval skills and wind vector errors, b) Distribution of derived wind direction solution closest to the true direction, (c) Comparison of algorithms' performances and errors under varying noise conditions

Apart from comparison of performance of NSDA and MLE algorithms across the inner beam swath, impact of noise on retrieval performance has also been studied. Figure (10c) depicts the comparison of performances and errors of NSD and MLE algorithms under varying noise conditions for all the WVC indicating similarity of these algorithms.

Thus, NSD algorithm is found be as good as MLE algorithm in respect of direction retrieval skill, wind vector errors and distribution of retrieved directions thus providing an alternative to MLE but with better computational efficiency. However, the errors in nadir regions are required to be improved using DIRTH algorithm developed by Stiles et al (2002).

5.2 Algorithm for directional ambiguity removal:

A block diagram of directional ambiguity removal algorithm is depicted in figure (11). The ambiguity removal algorithm utilizes all the vector solutions available from retrieval algorithm over the data locations within the swath and the ambiguity is removed based on the trend or the consensus of the rank-1 wind directions solutions over that area. In most of the cases, about over half of the rank-1 wind directions are found to be aligned in the true wind directional pattern under normal noise conditions while the remaining rank-1 directions are mostly in the opposite direction. A median filtering approach is used to remove directional ambiguities.

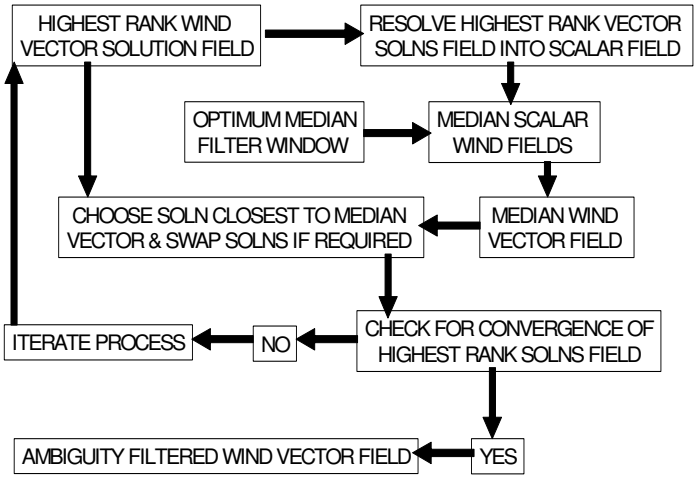

Figure 11: Block diagram of directional ambiguity removal algorithm

For this purpose, the rank-1 vectors over an area are first resolved into scalar components. With a moving window of optimized size, medians of both the scalars at each data location are determined using all the points falling within the window. The medians of respective scalars are used to find the median wind direction at each data location. Making use of median direction, all the direction solutions at that point are examined and the direction solution closest to median direction is identified and that vector is assigned as rank-1 solution swapping with its original ranking (Gohil, 1992). The procedure is followed for all the points in a scene cut out of the satellite pass and likewise the entire pass is processed. The filtering process for a scene is repeated in the above-mentioned manner till the entire processed wind field of that scene is converged. At this stage, the resulting wind field mostly resembles the true wind field in that scene.

It is important to note that the retrieval of ambiguity filtered wind vector field is mainly dependent on the amount of noise present in radar backscatter data as well as on its spatial distribution.

5.2.1 Algorithm for localized directional ambiguity removal:

In case when the scatterometer data is highly noisy over certain parts of the swath, the resulting wind field still may have localized ambiguities, which may not always be possible to be removed by the filtering process alone. Highly localized ambiguities may still be removed using a filtering process over coarser spatial resolution data prepared from the given data. In this method, the filtered wind field with localized ambiguities is further divided into small segments. Medians of the same ranking solutions for these coarser resolution data are obtained. The median solutions for these segments are further processed for ambiguity filtering as mentioned above. Based on filtered median wind field, the original ambiguity filtered wind field with localized ambiguity is corrected to yield final filtered wind field (Gohil and Pandey, 1994).

5.2.2 Directional ambiguity removal over inner beam swath:

The directional ambiguity removal over the inner beam swath may be performed in a usual manner as described above by first ignoring the wind solutions exactly over the sub-satellite track. Wind solutions over a very narrow region around sub-satellite track being very erroneous are firstly required to be ignored because of the retrieval skill halved

due to the symmetry of the measurement geometry and the pairing of solutions as mentioned in earlier sections. Subsequent to the ambiguity filtering in rest of the inner beam swath, wind solutions over the sub-satellite track should then be considered and the ambiguity filtering process should be repeated. This approach is crude. However, the DIRTH algorithm (Stiles et al, 2002) must be used for the purpose and its implementation is being worked out.

It is important to note that while using pencil-beam scatterometer, a narrow region of data swath centered at the sub-satellite track may have many data points with wind vector solutions not corresponding to the correct wind direction. This needs special processing and also requires external data like model surface analysis/forecast on operational basis. More so, in the outer region of the data swath where only two radar backscatter observations are available, the ranking of wind vector solutions becomes irrelevant while one of the solutions represents true wind direction. This also needs external data like numerical weather prediction model winds for ranking the solutions.

5.2.3 Directional ambiguity removal over exclusive outer beam swath:

Over the exclusive outer beam swath region where the backscatter measurements from only one beam but in two azimuth directions are available, the wind vector solutions do not have any meaningful ranking. Due to this reason, the derived solutions at all data locations are assigned rank-1 priority based on the model wind direction and are used along with inner beam solutions for ambiguity filtering through normal filter process as shown in block diagram of figure (12).

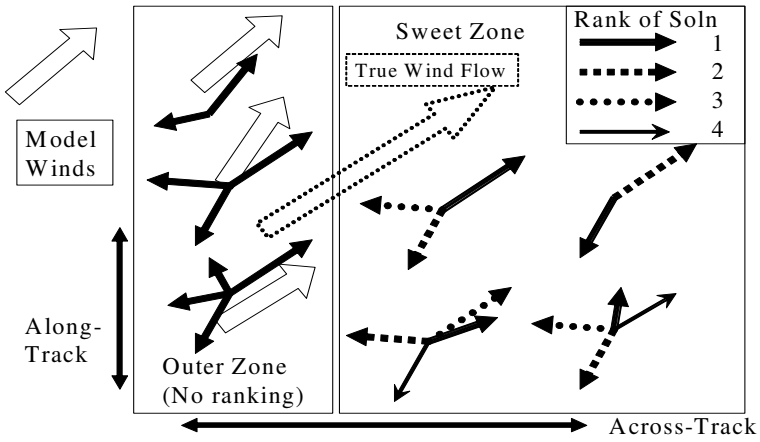

Figure 12: Role of model winds in tagging ranks to direction solutions over outer swath

In this process, certain weights are assigned to wind solutions depending upon its distance from the outer edge of the swath of inner beam, otherwise, ambiguity filter process will yield wind field more resembling to the model winds loosing the impact of measurements. Further details given by Stiles et al, (2002) are being worked out.

5.2.4 Testing of algorithms with Quikscat data:

The present algorithm has been tested with Quikscat data (MGDR NRT Version in BUFR format at 25 km spatial resolution) for one orbit (#29820) on March 11, 2005, at 12.00 GMT over inner beam swath only. Based on median filter, the directional ambiguity is removed using a two-step filtering at given and coarser spatial resolutions. Quikscat data derived wind fields using NSD and MLE algorithms are depicted in figures (13a) and (13b), respectively.

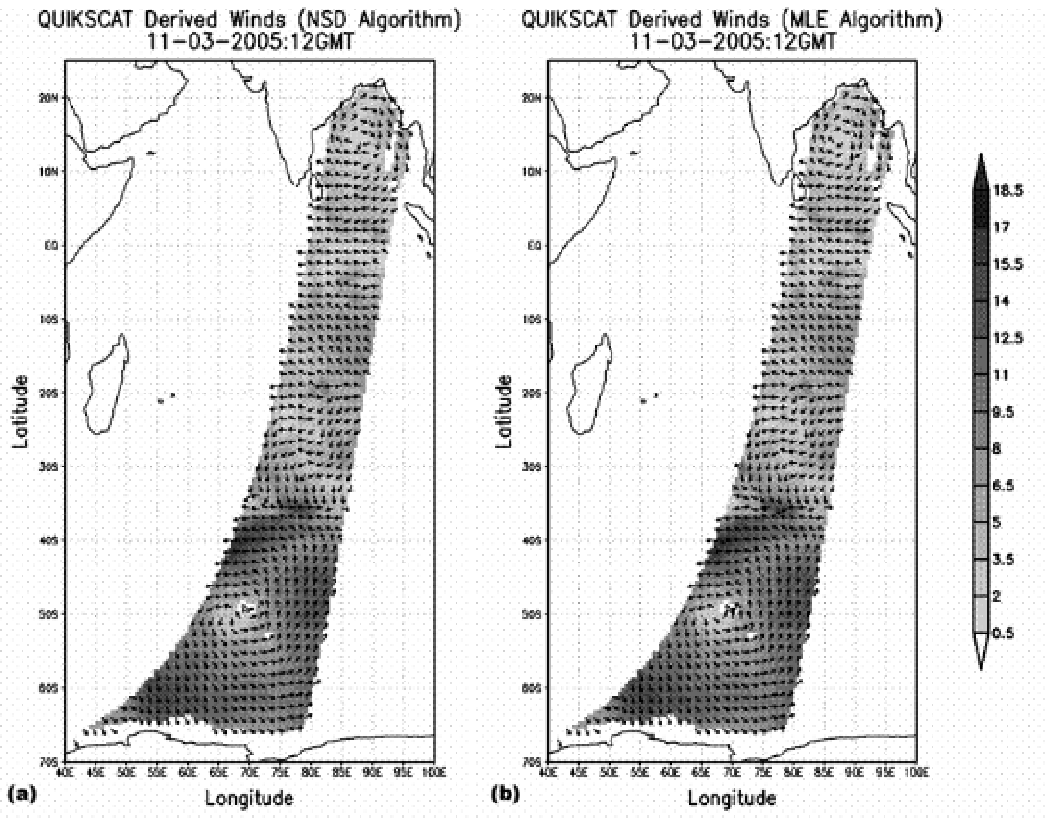

Figure 13: Ocean surface wind vector field derived from Quikscat radar backscatter data (NRT BUFR-25 km) over inner beam swath for March 11, 2005 over Indian region using, a) NSD algorithm, b) MLE algorithm

The derived winds are found to be very similar to each other as well with those of finished product winds (not depicted here). More so, the computational efficiency of the present algorithm is found to be higher (about 2 to 3 times) as compared to that of MLE algorithm during simulation studies as well as testing with Quikscat data (Gohil et al, 2006).

6.0 Flagging:

Retrieval of ocean surface wind vector from scatterometer is affected in the presence of rain due to modification of measured radar backscatter in two ways. During rain, the drops falling on water surface create crater, crown, stalk and ring waves. Out of these, ring waves contribute the most towards radar backscatter through Bragg resonance. Besides, rain attenuates the radar signal as well as contributes through volume backscattering. A study of rain impact on backscatter and associated wind vector retrieval is required for rain flagging of backscatter data.

Due to the directional symmetry of ring waves and the scattering from water drops in rain column the backscatter signals are depolarized causing diminishing difference of radar backscatter in vertical and horizontal polarizations. However, high intensity winds under rain-free conditions also lead to depolarization. The normalized polarization difference is found to have a potential for pre-retrieval rain flagging. Under moderate and high rain conditions, pre-retrieval rain flagging is feasible. Light rain and high wind conditions lead to false/missing rain flagging. The impact of rain is also observed in terms of drastic changes in retrieved wind speed and direction. Retrieval of wind vector under raining conditions is highly erroneous and mostly renders retrieval meaningless. This needs rain affected data to be ignored (or flagged out). In the present study, only rain flagging of data using the retrieval algorithm by Gohil et al (2006) has been attempted following procedures given by Portabella and Stoffelen (2001) yielding different success rates for rain-free and rainy conditions. The rain-flagging scheme has been tested with simulated data and the success rate of rain flagging under rain-free and rainy situations has been evaluated under different noise scenario. Under rain-free situations it is observed that the false reporting of rain cases is significantly low while for rainy cases, the missing rain events are, to some extent, high but are comparable with the studies made elsewhere. Spatial analysis of real data may further improve flagging.

6.1 Rain impact model and its development:

An empirical rain impact model for QuikSCAT to calculate rain affected radar backscatter over ocean is given by Draper and Long (2004) as

$$\sigma^0_m = \alpha_{rain}(\sigma^0_{wind} + \sigma^0_{rainstrike}) + \sigma^0_{rain} \quad (19)$$

Where σ^0_m is the measured Quikscat backscatter, σ^0_{wind} is the rain-free wind-induced radar backscatter, $\sigma^0_{rainstrike}$ is the surface backscatter perturbation due rain striking the ocean surface, α_{rain} is the two way atmospheric rain attenuation, and σ^0_{rain} is the volume scattering due to falling rain droplets. The model is further simplified by summing the attenuated surface perturbation and the atmosphere scattering terms, creating a single (lump) effective rain backscatter. The resultant rain impact model is

$$\sigma^0_m = \alpha_{rain}.\sigma^0_{wind} + \sigma^0_{rainy} \quad (20)$$

with

$$\alpha_{rain} = \sum_{k=0}^{2} A_k R^k \quad (21)$$

$$\sigma^0_{rain} = \sum_{k=0}^{2} S_k R^k \quad (22)$$

where R (km.mm/hr) is integrated rain rate. The σ^0_{wind} information is obtained from QSCAT-1 GMF for a known wind vector. Based on the above model, variations of atmospheric transmittance ($\tau=e^{-\alpha}$) and lump rain backscatter varying with integrated rain rate, for horizontal and vertical polarizations, are depicted in figure (14).

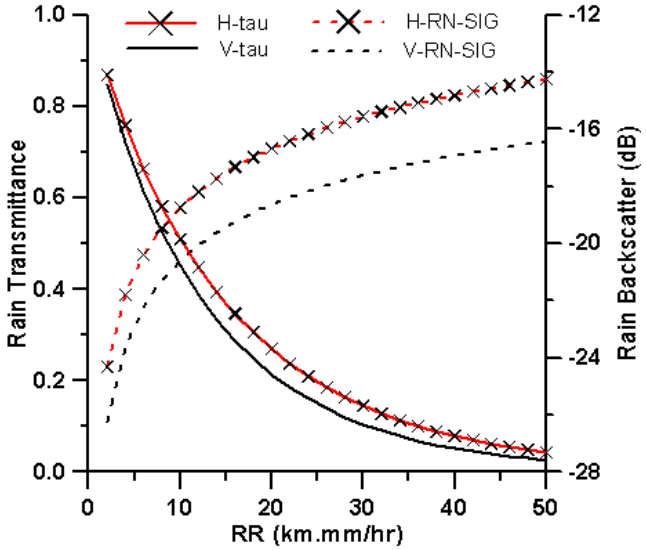

Figure (14): Variation of atmospheric transmittance (solid lines) and lump rain backscatter (dotted lines) with integrated rain for Quikscat scatterometer

It indicates that for both the polarizations, atmospheric transmittance nonlinearly decreases while lump rain backscatter nonlinearly increases with increasing rain rate. This empirical rain impact model is developed using simultaneously observed radar backscatter from Quikscat scatterometer, path integrated attenuation and rain rate profile from TRMM Precipitation Radar (PR), oceans surface wind vector from NCEP model analysis and the QSCAT-1 GMF. Development of such model specific to Oceansat-2 scatterometer will be essential in which radar backscatter data from Oceasat-2 scatterometer will be used along with rain and attenuation information from TRMM-PR and model wind data from ECMWF/NCEP. Prior to developing rain impact model, development of GMF specific to Oceansat-2 scatterometer will be necessary. The data requirements for rain impact model development are the same as reflected in table (3) with additional data of path-integrated attenuation from TRMM-PR.

6.2 Impact of rain on wind vector retrieval:

The impact of rain is studied through wind vectors retrieved by the method mentioned above by using simulated radar backscatter under rainy conditions obtained through equation (20). The impact of rain is observed in terms of drastic changes in retrieved wind speed and direction as shown in figures (15). The retrieved wind speed

below and above 15 m/s are over- and under- estimated, respectively as seen in figure (15a), while retrieved directions are aligned towards direction normal to sub-satellite track as observed in figure (15b). These observed characteristics under rainy conditions are utilized to flag the retrievals under rainy situations as mentioned subsequently.

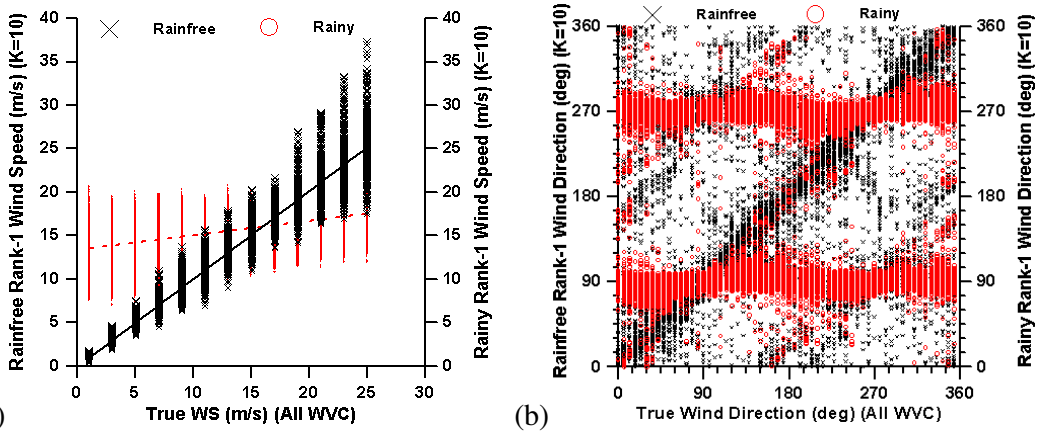

(a) (b)

Figure 15: Impact of rain on retrieval, (a) on retrieved speed, (b) on retrieved direction

6.3 Rain flagging:

Retrieval of wind vector under raining conditions is highly erroneous and is rendered meaningless. This needs rain affected data to be ignored (or flagged). Under very low intensity rain situations, winds can be retrieved with due corrections to backscatter through simultaneous retrieval of wind and rain using MLE (Draper and Long 2004a). Presently, only rain flagging of data using NSD algorithm has been attempted following the approach by Portabella and Stoffelen (2001) yielding different success rates for rain-free and rainy conditions. For rain flagging, the NSD values under rain-free and rainy situations have been compared keeping the observed behavior of the derived wind vectors in view. Rain rates from 0 to 50 km.mm/hr with an interval of 10 km.mm/hr are considered. The trends of variation of rank-1 SD values under rain-free and rainy conditions as shown in figure (16a) are found to be separable, hence, can be used for rain flagging. The SD values for rain-free and under low to moderate rain conditions are overlapping which primarily lead to such rain events undetected. However, apart from this, another useful clue used here is that the retrieved wind directions under rainy situations are mostly found to be around directions normal to the sub-satellite track. Thus a criterion is chosen to flag out possible raining situations in the data based on the above

information. The trends of wind speed binned mean and standard deviation of rank-1 SD with corresponding wind speed are established for all WVC as shown in figure (16b). The nonlinearly fitted mean and standard deviation of rank-1 SD are used for rain flagging (Portabella and Stoffelen, 2001). The rank-1 retrieved wind vector solution is assumed to be referring to raining condition if the following conditions are satisfied: 1) the retrieved wind speed WS^1_{PRCN} is above 7.0 m/s, 2) the difference of retrieved wind direction χ^1_{PRCN} with direction normal to sub-satellite track ($\Delta\chi^1_{PRCN}$) satisfies the condition $|Cos(\Delta\chi^1_{PRCN})| \leq 0.275$ and, 3) the difference of observed SD^1_{PRCN} and calculated rain-free SD_{RFAVG} satisfies the condition $\Delta SD^1_{PRCN} > 0.7.M_{SD}.SD_{RFSD}$, with $\Delta SD^1_{PRCN} = |SD^1_{PRCN} - SD_{RFAVG}|$, while SD_{RFAVG} and SD_{RFSD} are given by

$$SD_{RFAVG} = \Sigma_{Q=0}^{3} A_Q (WS^1_{PRCN})^Q \quad \text{and} \quad SD_{RFSD} = \Sigma_{Q=0}^{3} D_Q (WS^1_{PRCN})^Q \qquad (23)$$

where, A_Q and D_Q are the polynomial coefficients for average (solid line through "diamond" symbols) and standard deviation (dotted line through "plus" symbols) fitted curves of SD, respectively, as shown in figure (16b).

The fitted curves used for calculating SD_{RFAVG} and SD_{RFSD} are shown in figure (16b). The threshold multiplier M_{SD} varying from 1.8 to 2.2 is used for rain detection and has impact on rain detection under rain-free and rainy situations as shown in figure (16c). The above scheme has been tested with simulated data and the performance of rain flagging under rain-free and rainy situations has been evaluated as depicted in figure (16c). The overall proportionate success is a weighted success considering fractions of rain-free (about 90 percent) and rainy (about 10 percent) events at any given time over the globe as reported in literature (Portabella and Stoffelen, 2001; Stiles and Yueh, 2002; Draper and Long, 2004; Huddleston and Stiles, 2000). For no-rain situations it is observed that the false reporting of rain cases is significantly low while for raining cases, the missing rain events are, to some extent, high but are comparable with the studies made elsewhere (Portabella and Stoffelen, 2001; Huddleston and Stiles, 2000).

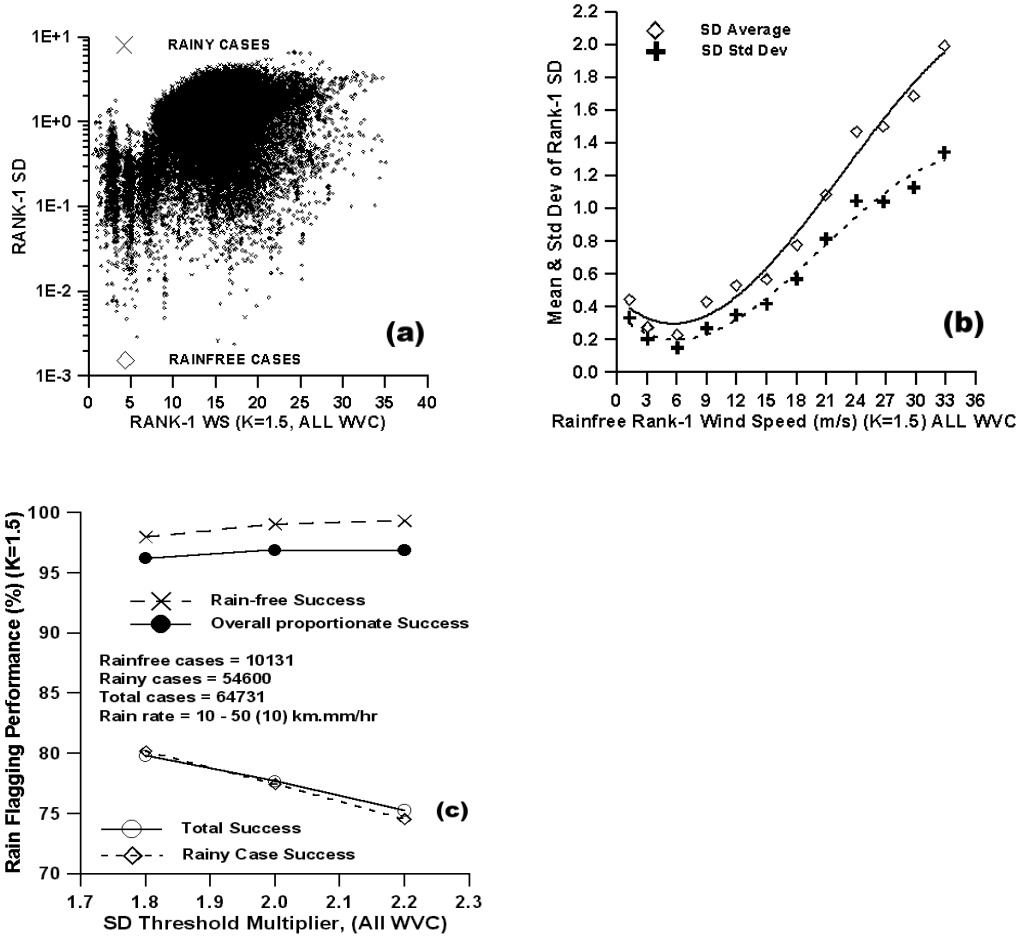

Figure (16): Rain flagging using NSD algorithm at K=1.5, a) Scatter plots of rank-1 SD and rank-1 wind speed under rain-free and rain conditions, b) Trends of rain-free mean and standard deviation of rank-1 SD for binned wind speed considering all WVC, c) Rain flagging performance for rain-free and rainy situations for different flagging thresholds.

6.4 Sea-ice flagging (Brief introduction):

Sea-ice altering the radar backscatter measurements affects the wind retrieval. The radar backscattered signal from the earth's surface is dependent on the roughness at the scale of the radar wave length, the incidence angle, and the dielectric properties of the surface, which for sea ice means ice salinity, temperature, air inclusion, liquid water fraction in snow and ice, and snow cover (Haarpaintner et al, 2004). At low wind speeds, horizontal polarization backscatter from the ocean is generally lower than backscatter

from ice but higher wind speed may produce ambiguities for ice-ocean discrimination because ice and ocean may exhibit similar mean backscatter values. Haarpaintner et al (2004) have given an approach (referred hereafter as HA) for sea-ice delineation making use of active polarization ratio (APR) and radar backscatter values. The APR is given as

$APR = (\sigma_{0H} - \sigma_{0V})/ (\sigma_{0H} + \sigma_{0V})$	24

Where σ_{0H}, σ_{0V} are radar backscatter on linear scale. Based on a number of criteria given in HA, the ice-flagging scheme is being considered for Oceanat-2 scatterometer. A limited number of criteria given in HA used here, are given in table (5).

Table 5: Ice-ocean thresholds

Parameter	Value
APR	>-0.02
σ_{0V}	>-25 dB
σ_{0H}	>-25 dB
Data satisfying these conditions is treated as ice	

Some of the results, on the basis of a limited criterion of HA, obtained from Quikscat radar backscatter products (BYU products) are presented here as a preliminary effort towards sea-ice flagging for Oceansat-2 (Rao, 2007). Shown in figure (17) are APR values obtained using Quikscat data for different dates during year 2000 indicating the presence of sea ice.

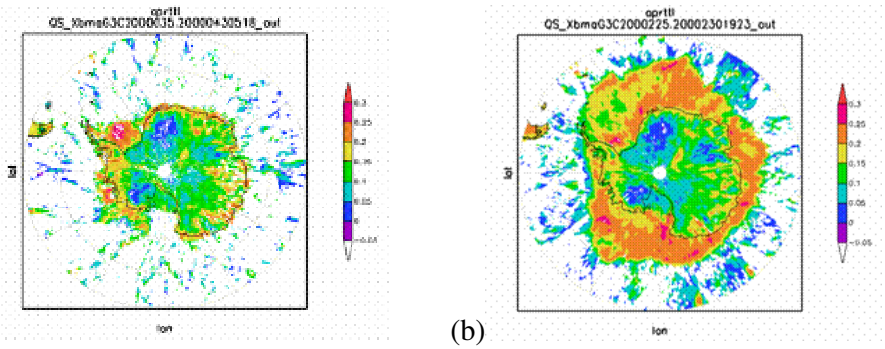

(a) (b)

Figure 17: Quikscat backscatter BYU product derived APR over Southern Polar region indicating sea-ice coverage for different dates (a) 11-02-2000, and (b) 17-08-2000

However, over ocean, some of the spurious data indicating sea-ice are also seen which may be due to higher winds as well as APR calculated at the edge of inner beam swath. Given here is only an introduction to the activity while detailed plan is being worked out separately (not a part of wind retrieval).

7.0 Initial phase validation:

This aspect to some extent is taken care during GMF development phase which will also include limited validation of GMF and the derived winds. However, calibration/validation activities are being pursued separately.

8.0 Limitations:

The major limitation is that the retrievals under cyclonic conditions are highly erroneous in terms of wind speed and direction as the cyclones are mostly associated with rain. This needs cyclonic data to be properly identified and processed in a proper manner taking care of rain (simultaneous retrievals). Apart from this, regions with highly variable wind fields like fronts, cols, vortices and others in the presence of large noise the directional ambiguities may not be properly filtered out. Due to different processes to be incorporated for outer and nadir regions, discontinuities in the direction fields may occur in some cases.

9.0 Acknowledgements

Authors wish to thank Dr. R. R. Navalgund, Director, Space Applications Centre (SAC), for his keen interest, encouragement and guidance. We thankfully acknowledge Dr. Ramrattan, Associate Director, SAC and Deputy Director, RESIPA, Dr. V.K. Agarwal, Group Director, MOG-RESIPA, and Dr. A. Sarkar, Head, OSD-MOG-RESIPA and Project Director OCEANSAT-II Utilization Program, for valuable suggestions on the document. Discussions with Dr. N.K. Vyas on sea-ice are thankfully acknowledged.

Authors would like to thankfully acknowledge NASA-JPL and NOAA for the Quikscat data and QSCAT-1 model functions used in studies reported in this document. ECMWF is thankfully acknowledged for making the BUFR data reading routines accessible. We wish to thank Drs. R.P. Sinha and Jeff Augenbaum associated to NOAA for their cooperation in providing sample Quikscat MGDR data and relevant information.

10.0 References:

1. Chi, C. and F.K. Li, (1988), "Comparative study of several wind estimation algorithms for spaceborne scatterometers", IEEE Tran. Geosci. Remote Sens., 26, pp. 115-12

2. Draper, D.W. and D.G. Long, (2004a), "Simultaneous wind and rain retrieval using SeaWinds data", IEEE Trans. Geosci. Remote Sens., vol 42, No.. 7, pp 1411-1423

3. Draper, D.W. and D.G. Long, (2004), "Evaluating the effect of rain on SeaWinds scatterometer measurements", J. Geophy. Res., Vol. 109, C02005, doi: 10.1029/20021C001741, pp. 1-12

4. Dunbar, S (1999), available online from http://aspera.jpl.nasa.gov/download/pub/ ocean_wind/quikscat/model_ function.

5. Fischer, R.E., (1972), "Standard deviation of scatterometer measurements from space", IEEE Trans. Geosci. Electronics, Vol. GE-10, No. 2, pp. 106-113

6. Gohil, B.S. and P.C. Pandey, (1985), "An algorithm for retrieval of oceanic wind vectors from the simulated SASS normalized radar cross-section measurements", J. Geophy. Res., Vol 90, No. C4, pp. 7307-7311

7. Gohil, B.S.,(1992), "Extraction of ocean surface wind field from simulated ERS-1 scatterometer data", International J. Remote Sensing, Vol 13, No. (17), pp. 3311-3327

8. Gohil, B.S. and P.C. Pandey, (1994), "A supplementary method for removing localised wind directional ambiguities in oceanic wind vector derived from ERS-1 scatterometer data", 15th Asian Conference on Remote Sensing, November 17-23, Bangalore

9. Gohil, B.S. and P.C. Pandey, (1995), "An atlas of surface wind vectors in the seas around India during August 1992 - July 1993 from ERS-1 scatterometer", Special Publication SP-76-95, ISRO-SAC-SP-76-95, Indian Space Research Organisation, Bangalore

10. Gohil, B.S., A. Sarkar, A.K. Varma and V.K. Agarwal, (2006), "Wind vector retrieval algorithm for Oceansat-2 scatterometer", Proc. SPIE, vol. 6410, doi: 0.1117/12.693563

11. Haarpaintner, J., R.T. Tonboe, D.G. Long, and M.L. Van Woert, (2004), "Automatic detection and validity of the sea-ice edge: An application of enhanced-resolution quikscat/ seawinds data", IEEE Trans. Geosci. Remote Sens, Vol. 42, No. 7, pp 1433-1443

12. Huddleston, J.N. and B.W. Stiles, (2000), "Multidimensional histogram rain-flagging technique for SeaWinds on QuikSCAT", Proc. IGARSS2000, vol. 3, pp. 1232-1234

13. Long, D.E. and J.M. Mendel, (1991), "Identifiability in wind estimation from wind scatterometer measurements", IEEE Trans. Geosci. Remote Sensing., 29(2), pp. 268-276

14. NASA, (2006), "QuikSCAT Science Data Product User's Manual, Overview & Geophysical Data Products", Version 3.0, D-18053 – Rev A, JPL, NASA, September

15. Oliphant, T.E. and D.G. Long, (1999), "Accuracy of scatterometer-derived winds using the Cramer-Rao Bound", IEEE Trans. Geosci. Remote Sen., vol. 37, No. 6, pp. 2642 – 2652

16. Pierson, W.J., (1989), "Probabilities and statistics for backscatter estimates obtained by a scatterometer", J. Geophy. Res., vol. 94, C7, pp. 9743-9759

17. Portabella, M. and A. Stoffelen, (2001), “Rain detection and quality control of SeaWinds”, J. Atmos. and Ocean Technol., Vol. 18, pp. 1171-1183

18. Rao, U.N., (2007), “Ice-flagging of Quikscat scatterometer data”, Report No. SAC/RESIPA/MOG/SR/04/2007, April.

19. SAC Report, (2005), “Oceansat-II scatterometer payload, Preliminary Design Review Document”, SAC/SCATT/PDR/01, October

20. Schroeder, L., D.H. Boggs, G. Dome, I.M. Halberstam, W.L. Jones, W.J. Pierson, and F.J. Wentz, (1982), "The Relationship Between the Wind Vector and the Normalized Radar Cross Section Used to Derive Seasat-A Satellite Scatterometer Winds," J. Geophys. Res., Vol. 87, No. C5, pp. 3318-3336

21. Stiles, B.W. and S.H. Yueh, (2002), “Impact of rain on spaceborne Ku-band wind scatterometer data”, IEEE Trans. Geosci. Remote Sensing, vol. 40, pp. 1973-1983

22. Stiles, B.W., B.D. Polland and R. S. Dunbar, (2002), “Direction interval retrieval with thresholded nudging: A method for improving the accuracy of QuikSCAT winds”, IEEE Trans. Geosci. Remote Sensing, 40(1), pp. 79-89

23. Stoffelen, A. and D. Anderson, (1997), “Scatterometer data interpretation: measurement space and inversion”, J. Atmos. and Ocean Technol., vol. 14(6), pp. 1298-1313

24. Stoffelen, A. and M. Portabella, (2006), “On Bayesian scatterometer wind inversion”, IEEE Trans. Geosci. Remote. Sensing, Vol. 44, No. 6, pp. 1523-1533

25. Tiwari, P. and B.S. Gohil, (2005), “Impact of empirical model function on retrieval of ocean surface wind vector from space-borne microwave scatterometer”, Report No. SAC/RESIPA/MOG/OSD/Oceansat-II/SR/01/2005, October

26. Ulaby, F.T., R. K. Moore, and A. K. Fung, (1981), “Microwave Remote Sensing -- Active and Passive”, Vols. 1 and 2, Addison-Wesley Pub. Co., Reading, Mass.

27. Wentz, F.J., S. Peteherych, and L.A. Thomas, (1984), "A Model Function for Ocean Radar Cross-sections at 14.6 GHz," J. Geophys. Res., Vol. 89, pp 3689-3704

28. Wentz, F.J. and D.K. Smith, (1999), “A model function for the ocean-normalized radar cross section at 14 GHz derived from NSCAT observations,” Jou. Geophys. Res., 104(C5), pp 11,499-11,514